

Lensing of 21cm Absorption “Halos” of $z \sim 20$ -30 First Galaxies

Pengjie Zhang^{1,2*}, Zheng Zheng^{3,4†} and Renyue Cen^{5‡}

¹ *Shanghai Astronomical Observatory, Chinese Academy of Sciences, 80 Nandan Road, Shanghai, China, 200030; pjzhang@shao.ac.cn*

² *Joint Institute for Galaxies and Cosmology (JOINGC) of SHAO and USTC*

³ *Institute for Advanced Study, Einstein Drive, Princeton, NJ 08540, USA; zhengz@ias.edu*

⁴ *Hubble Fellow*

⁵ *Princeton University Observatory, Princeton University, Princeton, NJ 08544, USA; cen@astro.princeton.edu*

16 October 2018

ABSTRACT

Extended 21cm absorption regions (dubbed “21cm absorption halos”) around first galaxies at $z \sim 30$ are likely the first distinctive structures accessible to radio observations. Though the radio array capable of detecting and resolving them must have $\sim 200 \text{ km}^2$ total collecting area, given the great impact of such detections to the understanding of the reionization process and cosmology, such radio survey would be extremely profitable. As an example, we point out a potentially useful byproduct of such survey. The resolved 21cm absorption “halos”, likely close to spherical, can serve as (almost) ideal sources for measuring the *cosmic shear* and mapping the matter distribution to $z \sim 30$. We investigate the expected lensing signal and consider a variety of noise contributions on the shear measurement. We find that $\text{S/N} \sim 1$ can be achieved for individual “halos”. Given millions of 21cm absorption “halos” across the sky, the total S/N will be comparable to traditional shear measurement of $\sim 10^9$ galaxies at $z \sim 1$.

Key words: cosmology: theory-cosmology:the large scale structure-gravitational lensing

1 INTRODUCTION

Gravitational lensing (see, e.g., reviews of Bartelmann & Schneider 2001; Refregier 2003) directly probes the matter distribution of the universe and is becoming one of the most important probes of cosmology. Gravitational lensing distorts galaxy shape (*cosmic shear*), changes galaxy number density (*cosmic magnification*) and induces mode-coupling in cosmic backgrounds. These observable lensing effects enable several powerful methods to extract cosmological information. Cosmic microwave background (CMB) lensing (Seljak & Zaldarriaga 1999; Zaldarriaga & Seljak 1999; Hu 2001; Hu & Okamoto 2002), 21cm background lensing (Cooray 2004; Pen 2004; Zahn & Zaldarriaga 2006; Mandel & Zaldarriaga 2006) and cosmic magnification measurements of 21cm emitting galaxies (Zhang & Pen 2005, 2006) are expected to achieve high signal-to-noise ratio (S/N) in the near future. On the other hand, cosmic shear measurements have achieved high S/N (e.g., Jarvis et al. 2006; Van Waerbeke et al. 2005; Hoekstra et al. 2006) and will be improved significantly by several ongoing or upcoming large lensing surveys.

Traditional cosmic shear measurements are fundamentally limited by intrinsic ellipticities of galaxies. Intrinsic

ellipticities have a dispersion $\sim 30\%$, much larger than the typical 1% lensing signal for source galaxies at $z = 1$. Even in the best case that ellipticities of galaxies do not correlate, one still needs to average over several hundred galaxies to achieve S/N of one. Furthermore, source galaxies at $z_s \gtrsim 3$ are difficult to detect optically, so it is hard to map the matter distribution at redshifts beyond 2 in optical lensing surveys. These two intrinsic problems can be overcome by the 21cm absorption regions around first galaxies (Cen 2006). These regions are of arc-minute size, or $\sim \text{Mpc}$ in comoving scale. Since their sizes are much larger than the nonlinear scale at corresponding redshifts, they are believed to be very close to spherical (Cen 2006). In addition, since they lie at redshifts $z \sim 25$, the lensing signal is strong. These two intrinsic advantages make these regions nearly ideal targets for shear measurement. Since these regions have distinctive structures, they are dubbed “21cm absorption halos” or “21cm halos”. We caution the readers that these 21cm “halos” are not virialized dark matter halos. In fact, the density fluctuations in these “halos” are well in the linear regime. In this paper, we study the requirement and application of the shear measurement of these 21cm “halos”.

Observations of 21cm absorption “halos” are challeng-

ing and are way beyond the capability of the planned square kilometer array (SKA¹). However, mission capable of resolving these “halos” will be extremely profitable. The 21cm brightness temperature can be simultaneously measured to high accuracy over a large fraction of the sky and a wide redshift range, without extra cost. This will allow the measurement of related statistics, such as the brightness temperature power spectrum, bispectrum, etc., to unprecedented accuracy and significantly improve our understanding on reionization process and cosmology at high redshifts. The detection of 21cm absorption “halos” will have potentially great impact on cosmology too (Cen 2006). Furthermore, the same mission can detect even smaller 21cm absorption regions around first stars, the so called Lyman- α spheres (because it is mainly the Lyman- α scattering that couples the 21cm spin temperature to the kinetic temperature, leading to the 21cm absorption against the CMB, Chen & Miralda-Escudé 2006), through strong lensing of galaxy clusters (Li et al. 2007). Given these potentially powerful applications, such mission deserve detailed investigation and observation efforts. In this paper, we discuss a surprisingly valuable byproduct of such mission: mapping the matter distribution to $z \sim 25$ through weak lensing of 21cm absorption “halos”.

As we show in this paper, the ellipticity induced by various contaminations is very likely to be controlled to below 10% for 21cm absorption regions considered here and we expect that shear measured from each such region would achieve $S/N \sim 1$. At $z \sim 25$ with $\Delta z = 2$, for a lower mass cut $\sim 7 \times 10^7 M_\odot$, the total number of these 21cm absorption “halos” is $\sim 10^6$ (Fig. 1). The total S/N will be equal to that with $\sim 10^9$ $z \sim 1$ source galaxies and thus comparable to what would be provided by planned ambitious cosmic shear surveys such as the Large Synoptic Survey Telescope².

Moreover, the lensing applications of 21cm absorption “halos” will fill the gap of source redshifts between traditional cosmic shear measurements (source redshifts $zs \leq 3$), cosmic magnification of 21cm emitting galaxies ($zs \sim 1\text{--}6$) and CMB lensing ($zs \simeq 1100$). They provide independent checks for 21cm background lensing ($zs \sim 10\text{--}30$).

Furthermore, lensing measurement to such high redshifts will provide a direct way of CMB delensing and improve the measurement of primordial inflationary gravitational waves (Sigurdson & Cooray 2005). Lensing reconstruction from 21cm absorption “halos” will significantly improve our understanding of matter distribution to $z \sim 25$ and the nature of dark matter, dark energy, gravity and inflation.

The paper is structured as follows. After a brief introduction of the 21cm absorption “halos” of first galaxies in § 2, we discuss their detection prospect in § 3. Then, in § 4 we define the mean cosmic shear to be measured for these “halos”. It would be ideal for cosmic shear measurement if the 21cm “halos” are intrinsically spherical. Therefore, in § 5, by investigating several sources that may induce ellipticity of these “halos”, we estimate the expected ellipticity and show that these regions are quite close to spherical. Given the expected noise, in § 6 we show the range of lensing power

spectrum that can be precisely measured. Finally, we summarize and discuss the main results. Throughout the paper, we assume a spatially flat Λ CDM cosmology with matter density parameter $\Omega_m = 0.26$, baryon density parameter $\Omega_b = 0.044$, primordial power index $ns = 0.95$, Hubble constant $H_0 = 100h = 72 \text{ km s}^{-1} \text{ Mpc}^{-1}$, and a fluctuation amplitude $\sigma_8 = 0.77$ on $8 \text{ h}^{-1} \text{ Mpc}$ scales, which is consistent with the Wilkinson Microwave Anisotropy Probe (WMAP) three-year results (Spergel et al. 2006). For some plots, we also show cases with $\sigma_8 = 0.9$.

2 21CM ABSORPTION “HALOS” OF FIRST GALAXIES

Since the standard cold dark matter (CDM) cosmological model is by now accurately determined (Spergel et al. 2006), one could make testable predictions for the first generation of galaxies, expected to form within halos of mass $M = 10^5\text{--}10^9 M_\odot$ at $z = 20\text{--}40$ (Fig. 1). The first galaxies are expected to be small and faint in terms of stellar optical light. The very first galaxies may have masses of $\sim 10^5 M_\odot$ (Peebles 1980), limited by Jeans mass and molecular hydrogen cooling. However, star formation in minihalos with molecular cooling might be quenched, when hydrogen molecules are destroyed by Lyman-Werner photons. In any case, because of the expected low star formation efficiency in the minihalos, their 21 cm signals will be too weak to be relevant even if they form stars. However, as shown in Cen (2006), with the coupling of the 21cm spin temperature to Lyman- α scattering, some of the large first galaxies with total mass $M \geq 10^{7.5} M_\odot$ may each display an extended hydrogen 21cm absorption “halo” against the cosmic microwave background with a brightness temperature decrement of $\delta T = -(100\text{--}150) \text{ mK}$ at a radius of $0.3\text{--}3.0 \text{ Mpc}$ (comoving), corresponding to an angular size of $10\text{--}100 \text{ arcseconds}$. These large galaxies can cool by atomic processes.

The detection of these radio “halos” around first galaxies will be extremely profitable, although admittedly difficult. If and when a 21cm radio survey of first galaxies is carried out, some fundamental applications for cosmology and galaxy formation may be launched, as discussed in Cen (2006). Here, we recapitulate them. First, it may yield direct information on star formation physics in first galaxies. Second, it could provide a unique and sensitive probe of small-scale power in the standard cosmological model hence physics of dark matter and inflation, by being able to, for example, constrain the primordial power index ns to an accuracy of $\Delta ns = 0.01$ at a high confidence level. Constraints on the nature of dark matter particles, i.e., mass or temperature, or running of index could be still tighter. Third, clustering of galaxies that may be computed with such a survey will provide an independent set of characterizations of potentially interesting features on large scales in the power spectrum including the baryonic oscillations, which may be compared to local measurements (Eisenstein et al. 2005) to shed light on gravitational growth and other involved processes from $z = 30$ to $z = 0$. Finally, the 21cm absorption halos are expected to be highly spherical and trace the Hubble flow faithfully, and thus are ideal systems for an application of the Alcock-Paczyński test (Alcock & Paczyński 1979). Exceedingly accurate determinations of key cosmo-

¹ <http://www.skatelescope.org/>

² LSST: <http://www.lsst.org/>

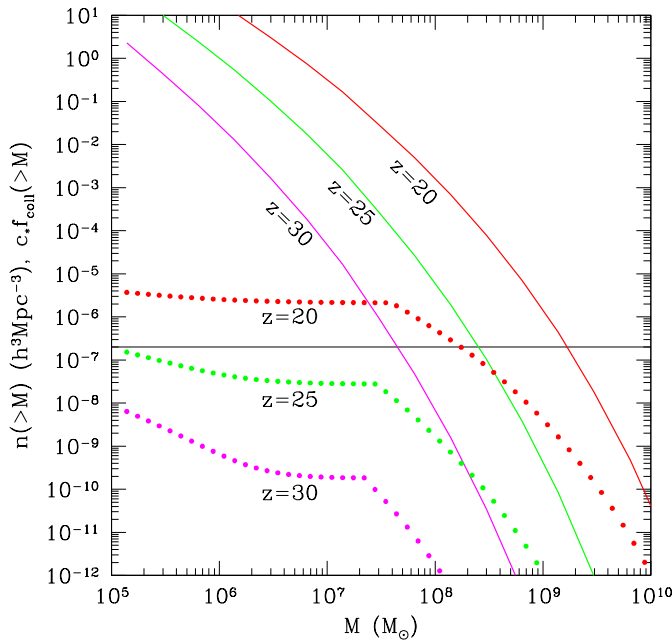


Figure 1. Solid curves are cumulative halo mass functions at $z = 30, 25$, and 20 (bottom up), predicted by the Sheth-Tormen formula (Sheth & Tormen 2002). Dotted curves are products of the star formation efficiency c^* and the fraction f_{coll} of matter that has collapsed to halos where stars have formed at the three redshifts. The horizontal line represents a threshold value of $c^* f_{\text{coll}}$, below which the heating of the IGM by the X-ray background is not significant, with a temperature increment less than $\sim 2\text{K}$ (Cen 2006). This figure is a reproduction of Fig.3 in Cen (2006) using the more accurate Sheth-Tormen mass function, assuming $c^* = 0.2$ (0.001) for large halos (minihalos), and adopting cosmological parameters consistent with WMAP three-year results (Spergel et al. 2006), $\Omega m = 0.26$, $\Omega \Lambda = 0.74$, $\Omega b = 0.044$, $h = 0.72$, $\sigma 8 = 0.77$ and $n s = 0.95$. We focus on halos with mass greater than $\sim 7 \times 10^7 M_\odot$, which could harbor first galaxies capable of producing extended 21cm absorption regions against CMB (Cen 2006).

logical parameters, in particular, the equation of state of the dark energy, may be finally realized. As an example, it does not seem excessively difficult to determine the dark energy equation of state w to an accuracy of $\Delta w \sim 0.01$, if Ωm has been determined to a high accuracy by different means. If achieved, it may have profound ramifications pertaining dark energy and fundamental particle physics (e.g., Upadhye et al. 2005). This last property may also make them ideal sources for weak gravitational lensing measurements, as investigated here.

3 DETECTABILITY

The resolution and r.m.s. noise of a radio survey depend on the detailed array configuration. Without loss of generality, we focus on a configuration of $N \times N$ arrays homogeneously distributed over a square with side length L . The resolution is $\theta p = \sqrt{\pi \alpha^2 / 4\lambda} / L$, where $\alpha \simeq 1.2$ for this specific configuration and $\lambda = 0.21(1+z)\text{m}$ is the redshifted wavelength of the 21cm line. Foreground contaminations at the

low frequencies of concern here are overwhelming. The dominant one is galactic synchrotron emission, which scales as ν^β with $\beta \sim -2.55$. For concreteness, we adopt the brightness temperature at $\nu \sim 54\text{MHz}$ (redshifted frequency of the 21cm lines at $z = 25$) as $T^{\text{syn}} b \simeq 3000\text{ K}$. This number is consistent with Keshet et al. (2004) and Chen & Miralda-Escudé (2006). However, brightness temperature estimation at these low frequencies is quite uncertain (e.g., $T^{\text{syn}} b$ adopted by Bowman et al. 2006 is a factor of 2 higher, if scaled to $z = 25$). A factor of 2 increase in $T^{\text{syn}} b$ would require a factor of 4 increase in integration time or a factor of 2 increase in the total collecting area, in order to achieve the same S/N.

Since the foreground is highly smooth in frequency space and the 21cm signal has line features, showing as sharp fluctuations in the spectrum, the mean foreground contamination can be efficiently removed pixel by pixel (Wang et al. 2006). The residual noise per resolution pixel (with area θp^2) caused by photon number fluctuations in foreground and instrumental noise can be worked out to be (Thompson et al. 2001)

$$\begin{aligned} \sigma T &\simeq \frac{T_{\text{sys}}}{\sqrt{\Delta\nu} \pi \alpha^2 f_{\text{cover}}} \frac{4\sqrt{2}}{} \\ &\simeq 10 \text{ mK} \frac{T_{\text{sys}}}{3000\text{K}} \left(\frac{\Delta\nu}{300\text{kHz}} \frac{t}{1\text{year}} \right)^{-1/2} \left(\frac{f_{\text{cover}}}{14\%} \right)^{-1}. \end{aligned} \quad (1)$$

Here, $f_{\text{cover}} = A_{\text{total}} / L^2 = N^2 A_{\text{dish}} / L^2$ and A_{dish} is the collecting area of each dish. The bandwidth $\Delta\nu$ is related to the comoving separation r by $\Delta\nu \simeq 46\text{kHz} [26/(1+z)]^{1/2} [r/h^{-1}\text{Mpc}]$. The typical bandwidth $\Delta\nu = 300\text{kHz}$ corresponds to $\sim 6h^{-1}\text{Mpc}$ (comoving) at $z \sim 25$, which is about the diameter of the 21cm absorption “halos” (see Fig. 2). The integration time t per pixel is also the integration time per field of view (FOV). The system temperature $T_{\text{sys}} \simeq T b^{\text{syn}}$ in our case. We note that the noise estimate is much larger than that from the Poisson noise of photons. The reason is simple — in the Rayleigh-Jeans part of the emission spectrum, the mean occupation number \bar{n} of photons per quantum state is much greater than unity and the variance, which is $\bar{n}(\bar{n} + 1)$, is super-Poisson.

With assumptions on the star formation properties in the central sources, the brightness temperature profile of the 21cm absorption “halos” can be computed (see Cen 2006 for details). At $z = 25$, 21cm absorbing regions generated by first galaxies in $10^8 M_\odot$ halos have angular size of several arc-minutes with signal $\lesssim -50\text{mK}$ (top panels, Fig. 2). To reliably measure the shape of these “halos”, a resolution of $\theta p \sim 0.3'$ and a system temperature noise $\sigma T \sim 10\text{mK}$ are required. For $\Delta\nu = 300\text{kHz}$ and $f_{\text{cover}} = 14\%$, this translates to $L \sim 40\text{ km}$, $A_{\text{total}} \sim 200\text{km}^2$, and an integration time of one year per FOV. Detecting such regions at 5σ level without resolving them is relatively easy, which requires $L \sim 4\text{ km}$ and $A_{\text{total}} \sim 2\text{ km}^2$. The FOV at these wavelengths is typically $\sim 10^3 \text{ deg}^2$. To cover the whole sky, the total integration time of the order of half a century is required. Clearly, resolving these 21cm “halos” is not doable in the near future without major technological breakthrough or significant improvement in financial resources. Still, the theoretical merit of this study remains and could be useful for mid and far future proposals on dark age science.

The signal and size of the 21cm absorption “halos” do

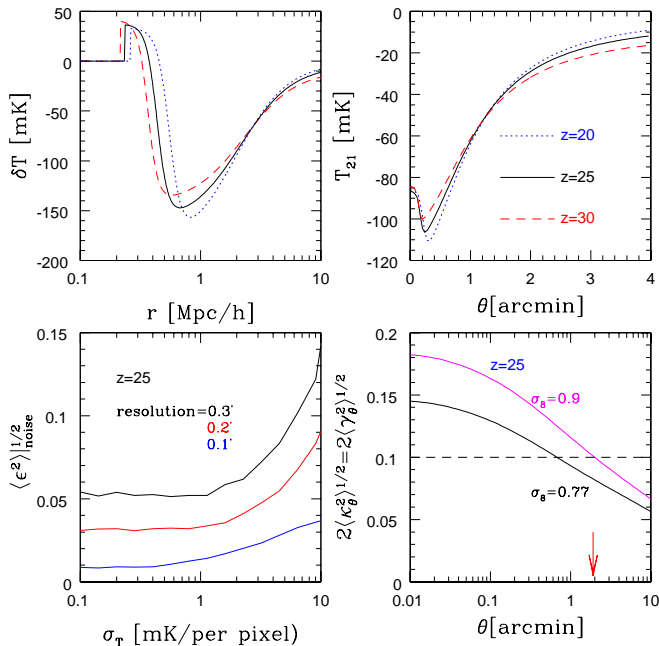


Figure 2. Top left panel: the brightness temperature of a 21cm absorption “halo” as a function of radius (in comoving unit), around a first galaxy in a $10^8 M_\odot$ halo at $z = 30, 25, 20$, respectively. The star formation efficiency $c_* = 0.2$ is adopted. Top right panel: the brightness temperature averaged over $\pm 3h^{-1}\text{Mpc}$ (comoving) along the line of sight. At these redshifts, 1 arcminute corresponds to $\simeq 2.4h^{-1}\text{Mpc}$ (comoving). Bottom left panel: ellipticities caused by random system noise (with an r.m.s. σ_T per resolution pixel). See the text for details. Bottom right panel: the lensing signal, κ or γ , smoothed over an area θ^2 . The arrow denotes the size of the 21cm absorption regions used for shear measurement. The dashed line is roughly the expected noise level.

not have strong dependence on the redshift (Fig. 2), until X-ray heating becomes important. However, towards higher redshifts (e.g., $z = 30$), thus lower frequency for observation, the foreground increases significantly. Detecting and resolving these regions at $z = 30$ would require more ambitious surveys. Furthermore, the number of halos drops by a factor of ~ 100 from $z = 25$ to $z = 30$ (Fig. 1), which substantially reduces the significance of shear measurement at $z = 30$. These factors make the measurement of shear for $z = 30$ “halos” very unlikely. Towards lower redshifts, the shear measurement is also unlikely, but for a different reason. One necessary condition for the existence of the 21cm absorption feature around the first galaxies is that the intergalactic medium (IGM) is not significantly heated by the X-ray background. We recast the arguments in Cen (2006) by using the more accurate halo mass function (Sheth & Tormen 2002) and adopting cosmological parameters consistent with WMAP three-year results (Spergel et al. 2006). The results are shown in Figure 1, and we find that the above condition can be satisfied at $z \gtrsim 23$. Therefore, we will focus our study for $z = 25$.

4 COSMIC SHEAR

To estimate the feasibility of shear measurement from 21cm absorption “halos”, we make several simplifications. We assume the dishes to distribute homogeneously in a square. This results in a homogeneous u - v sampling and alleviates the work involved in map making. This allows us to follow the usual cosmic shear measurement strategy and work in the real space. Real survey configurations often result in inhomogeneous u - v sampling and induced systematics in map making inevitably. However, Chang et al. (2004) show that these systematics can be corrected. Furthermore, the shapelet method, which directly works in the u - v space, is shown to be successful (Chang et al. 2004) and should be applied for real data. For these reasons, we neglect these systematics in our estimation.

Since the measurement noise is often large, we do not try tomography in frequency space for each 21cm absorption “halo”. We average the measurements along the line of sight over each “halo” and define the averaged brightness temperature along the line of sight $T_{21} = \int (dI/\partial T)\delta T d\nu / [\partial I/\partial T \Delta\nu] \simeq \int \delta T d\nu / \Delta\nu$. Here, I is the CMB intensity and $(\partial I/\partial T)\delta T$ is the associated CMB intensity decrement caused by 21cm absorption. The estimation shown here is by no means optimal and S/N could be improved by more advanced methods.

The two orthogonal components of the ellipticity ϵ of a 21cm absorption “halo” are given by the estimator

$$\epsilon_1 = \frac{Q_{11} - Q_{22}}{Q_{11} + Q_{22}}, \quad \epsilon_2 = \frac{2Q_{12}}{Q_{11} + Q_{22}}. \quad (2)$$

The quadrupole moments Q_{ij} are defined by

$$Q_{ij} \equiv \frac{\int qT[T_{21}(\theta)]\theta i\theta j d^2\theta}{\int qT[T_{21}(\theta)]d^2\theta}, \quad (3)$$

where $qT(T_{21})$ is a weighting function. We choose $qT(T_{21}) = T_{21}$ when $T_{21} < T_{\text{th}}$ and $qT = 0$ otherwise, and T_{th} is a threshold of brightness temperature that defines the boundary of each region used for shear measurement. The position θ is measured with respect to the center with $i, j = 1, 2$ the two orthogonal directions. For a round object, ϵ is induced by the cosmic shear and we have

$$\epsilon = \frac{2\gamma}{1 - \kappa + \gamma^2/(1 - \kappa)} \simeq \frac{2\gamma}{1 - \kappa} \equiv g \simeq 2\gamma. \quad (4)$$

Here, γ and κ are the lensing shear and convergence, respectively. With the presence of the ellipticity ϵN induced by other sources (see § 5), we have $\epsilon \simeq \epsilon N + 2\gamma$. In equation (4), we have approximated the reduced shear $g \simeq 2\gamma$ since in general $\kappa \ll 1$. The second order term $\kappa\gamma$ in g has a 1-10% contribution to the power spectrum (Dodelson et al. 2006), which slightly improves the detectability. However, given the uncertainties in ϵN , we neglect this higher order correction.

An implicit assumption of the estimator (eq. 4) is that cosmic shear does not vary across the integral area. This assumption holds closely for galaxies, which are of arc-second size. The 21cm absorption “halos” are of arc-minute size and the cosmic shear does vary across these regions. In this case, the estimator (eq. 4) measures the averaged cosmic shear. Higher order moments can be explored to extract the gradient of the cosmic shear (e.g., Goldberg & Bacon 2005). The relatively large size of 21cm absorption “halos” could

improve the S/N of such measurements. In this paper, we only discuss the mean shear signal of each 21cm absorption “halo”.

5 STATISTICAL ERRORS

Both the system temperature noise and inhomogeneities in neutral hydrogen density³ and spin temperature induce effective ellipticity ϵN to 21cm absorption regions. This ϵN has expectation value zero and does not correlate over large distance. Analogous to galaxy intrinsic ellipticity, it only induces shot noise to the shear measurement. Since inhomogeneities and anisotropies in spin temperature, if exist, are mainly caused by the central source, they are uncorrelated with inhomogeneities in neutral hydrogen density. The r.m.s. fluctuation in ϵN then has three independent contributions:

$$\sigma^2 \epsilon \equiv \langle \epsilon N^2 \rangle = \langle \epsilon^2 \rangle |\text{noise} + \langle \epsilon^2 \rangle |\delta H + \langle \epsilon^2 \rangle |Ts, \quad (5)$$

where $\langle \epsilon^2 \rangle |\text{noise}$, $\langle \epsilon^2 \rangle |\delta H$, and $\langle \epsilon^2 \rangle |Ts$ are ellipticity fluctuations caused by the system temperature noise, the inhomogeneity in the neutral hydrogen distribution, and the anisotropic distribution of the spin temperature around the first galaxies, respectively.

5.1 Ellipticity induced by the noise in system temperature

The distribution of the system temperature noise is Gaussian with an r.m.s. σT given by equation (1). To estimate the fluctuation $\langle \epsilon^2 \rangle |\text{noise}$ in the ellipticity induced by this noise, we generate a series of realizations of observations by adding Gaussian noise with an r.m.s. fluctuation σT to the otherwise spherically distributed signal and measure the ellipticity using equation (2). The result is shown in the bottom left panel of Figure 2. For $\sigma T \sim 10\text{mK}$ and resolution $0.3'$, the induced ellipticity is $\sim 10\%$ for $z = 25$. To have $\langle \epsilon^2 \rangle |\text{noise}^{1/2} < 0.1$, $\sigma T < 7\text{ mK}$ is required. This translates to a total collecting area $\gtrsim 300\text{ km}^2$ for $L = 40\text{ km}$. The induced ellipticities at other redshifts (e.g., $z = 20$ or 30) are similar, due to their similar signals (Fig. 2).

We notice that even for $\sigma T \rightarrow 0$, $\langle \epsilon^2 \rangle |\text{noise}$ does not vanish, rather it reaches a plateau instead. This is caused by the limited spatial resolution. With a finite resolution, one can not exactly identify the physical center of each regions, and any shift from the physical center would result in an effective ellipticity. As shown in the bottom left panel of Figure 2, with fixed σT , one can indeed reduce $\langle \epsilon^2 \rangle |\text{noise}$ significantly by improving the angular resolution θ_p . However, in reality, the requirement to improve resolution is often in conflict with the requirement to reduce the noise. To improve the angular resolution, longer base line is required ($\theta_p \propto L^{-1}$). If the total collecting area is fixed, f_{cover} would decrease ($f_{\text{cover}} \propto L^{-2}$). This would cause the noise σT (per resolution pixel) to increase ($\sigma T \propto f^{-1} \text{cover} \propto L^2 \propto \theta_p^{-2}$) and $\langle \epsilon^2 \rangle |\text{noise}$ to increase as well (Fig. 2). Therefore, improving angular resolution does not necessarily reduce errors in

shear measurement, unless the total collecting area is increased accordingly. Optimal surveys may balance between the angular resolution and σT to reduce $\langle \epsilon^2 \rangle |\text{noise}^{1/2}$ to a level well below the intrinsic ellipticity induced by the spin temperature anisotropy (§5.3).

5.2 Ellipticity induced by density inhomogeneities

The fluctuation $\langle \epsilon^2 \rangle |\delta H$ in the ellipticity induced by inhomogeneities in neutral hydrogen density can be estimated as

$$\langle \epsilon^2 \rangle \delta H \simeq \left[\int qT\theta^2 d^2\theta \right]^{-2} \times \int qT(T21)qT(T21')w(\theta - \theta') \times [(\theta 1^2 - \theta 2^2)(\theta 1'^2 - \theta 2'^2) + 4\theta 1\theta 2\theta 1'\theta 2'] d^2\theta d^2\theta' \quad (6)$$

Here, $w(\theta)$ is the angular correlation function of the neutral hydrogen over-density. In this expression, we have neglected fluctuations in the denominator $Q11 + Q22$ (eq. 2) since they only cause second order effect, due to non-vanishing $Q11 + Q22$. For a flat $w(\theta)$, $\langle \epsilon^2 \rangle |\delta H$ vanishes due to the geometry terms in equation (6). In reality, $w(\theta)$ varies slowly. So $w(\theta)$ does not contribute much to the integral in equation (6), although itself can reach $\sim 10^{-2}$ at sub arc-minute scale. For a 21cm absorption “halo” of a galaxy in a $10^8 M_\odot$ halo at $z = 25$, $\langle \epsilon^2 \rangle |\delta H < 10^{-4} \ll 4\langle \gamma^2 \rangle$ for $T_{\text{th}} \sim -50\text{mK}$. Therefore, this source of error seems to be negligible.

First galaxies are more likely to reside in high density regions and one may think that this strong formation bias invalidates the above conclusion, which is based on the ensemble average of the correlation function. As the shear measurement only depends on the variation in the local density field, to account for the environmental effect, one should replace $w(\theta)$ in equation (6) with the conditional correlation function $w(\theta|\langle \delta H \rangle)$, where $\langle \delta H \rangle$ is the overdensity averaged over the 21cm absorption regions for shear measurement. Being several Mpc/h in size, these regions are much larger than the nonlinear scale or filament size at $z \sim 25$, which implies that $\langle \delta H \rangle \ll 1$. Hence we do not expect that $w(\theta|\langle \delta H \rangle) \gg w(\theta)$. On the other hand, even if $w(\theta|\langle \delta H \rangle)$ could be 10 times larger than $w(\theta)$, the induced $\langle \epsilon^2 \rangle |\delta H^{1/2}$ would be still less than 3%. Based on these arguments, we conclude that the ellipticity induced by inhomogeneities in neutral hydrogen density, if not negligible, is at most subdominant to other error sources.

5.3 Ellipticity induced by spin temperature inhomogeneities

The fluctuation $\langle \epsilon^2 \rangle |Ts$ in the ellipticity induced by anisotropies in the spin temperature distribution is most uncertain. The spin temperature is a weighted average of the CMB temperature and the gas kinetic temperature. For the temperature range in our study, the CMB temperature is perfectly homogeneous. The coupling coefficients of the spin temperature to the gas temperature are determined by the spin-changing collisional rate and the Lyman- α scattering rate (Wouthuysen 1952; Field 1959). On scales we consider, the collisional rate should be isotropic because of isotropic distributions of the gas temperature and density. However, the spatial distribution of the Lyman- α scattering

³ Peculiar velocities are highly coherent across the 21cm absorption region, so it is unlikely to induce a non-negligible ellipticity.

rate highly depends on the origin and propagation of Lyman- α photons, which could introduce considerable anisotropies in the spin temperature distribution.

Cen (2006) considers Lyman- α photons originated from the galaxy at the center of each halo. Photons blueward Lyman- α from the continuum of Population III stars in the galaxy redshift to the Lyman- α line-center frequency because of the Hubble expansion. At the radius where a blue photon redshifts to Lyman- α frequency, the photon is continuously scattered by neutral hydrogen atoms in the IGM and has little spatial diffusion. The photon would not fly freely until it encounters an atom that has the right velocity to make a large jump in its frequency. The escape of photons slightly blueward the Lyman- α line-center frequency from the central galaxy is affected by the neutral hydrogen distribution near the center. If the neutral hydrogen column density in the innermost 1kpc of the halo is above 10^{17}cm^2 (which is highly possible) and the column density distribution is not isotropic (e.g., caused by the geometry of the star forming region or the galactic wind), it would lead to anisotropic distributions of the Lyman- α scattering rate and the spin temperature at large radii.

However, before a photon reaches the radius where it redshifts to Lyman- α and becomes strongly scattered, there is a probability for it to be scattered and thus change its propagation direction. The place where the photon encounters a tremendous number of scatterings with little spatial diffusion is then no longer along the initial direction that the photon escapes from the central galaxy. Therefore, a small number of scatterings encountered by photons before they reach the region where strong scatterings happen tend to make the distribution of the overall scattering rate more isotropic than the initial angular distribution of the photons from the central galaxy.

To quantify such an effect of isotropization, we simulate the Lyman- α scattering process around the galaxy using a Monte Carlo code (Zheng & Miralda-Escudé 2002). Photons near Lyman- α frequency are launched from the center along a cone with a given open angle to represent the anisotropic initial distribution. Every scattering of a photon is followed until the photon escapes to infinity. The scattering rate at each position in the IGM around the galaxy is then obtained with its normalization set by the luminosity of the central galaxy around Lyman- α frequency (see Cen 2006). We calculate the resultant spin temperature distribution and find that with a threshold $T_{\text{th}} = -50\text{mK}$ of the 21cm absorption region, the ellipticity fluctuation $\langle\epsilon^2\rangle|Ts^{1/2}$ introduced by the initial anisotropic Lyman- α emission are 0.21, 0.20, 0.16, 0.14, 0.08, and 0.03 for open angles of 5° , 15° , 30° , 45° , 60° , and 75° , respectively. We may expect that galaxy formation at such high redshifts is quite irregular and thus the formation of a well defined disk is unlikely. If this is the case, it may be unlikely that the effective open angles are much smaller than $\sim 30^\circ$. But even in such extreme cases, a small number of initial scatterings are quite efficient in isotropizing the final scattering rate distribution by making most resonant scatterings happen at a position along a direction deviating from the initial one.

The situation may be even more optimistic than the above estimates. Besides photons originally emitted slightly blueward the Lyman- α frequency that redshift to the Lyman- α frequency, there are other sources of Lyman- α

photons that can contribute to the pumping rate of the 21cm line. Photons originally emitted between Lyman- γ and Lyman limit can redshift into one of the higher Lyman series resonance, and, after a few scatterings, cascade to locally produce Lyman- α photons near the line center (Chuzhoy et al. 2006; Chuzhoy & Shapiro 2006). Owing to the lower cross-section of the photons between Lyman- γ and Lyman limit, they are expected to escape from the central galaxy more isotropically than those slightly blueward Lyman- α . The small number of scatterings before they cascade to produce Lyman- α photons would further isotropize the distribution. Another source of Lyman- α photons is from soft X-ray photons. Chen & Miralda-Escudé (2006) discuss 21cm absorption halos around first stars and argue that soft X-ray photons from Population III stars play a significant role in (collisionally) generating Lyman- α photons. These Lyman- α photons produced locally in the inner IGM region surrounding the galaxy are likely to be largely isotropic because of the largely isotropic escape of soft X-ray photons from the galaxy.

Based on the above investigation, we conclude that the ellipticity induced by the anisotropies in the spin temperature is likely at the level of $\lesssim 0.1$ but may be much smaller. Depending on the nature of these objects and observation configurations, either the noise induced ellipticity or the spin temperature induced ellipticity can dominate the error budget of shear measurement. The overall induced ellipticity is thus expected to be $\lesssim 10\%$ but could be smaller.

6 LENSING MEASUREMENTS

The lensing signal on arc-minute scales at $z = 25$ is $2\kappa \sim 10\%$ (lower right panel, Fig. 2). From the previous section, the expected noise is likely $\lesssim 10\%$. We then expect that the S/N of the shear measurement for each 21cm absorption “halo” is ~ 1 . This S/N is impressive, comparing to $\text{S/N} \sim 1/30$ of the conventional shear measurement of optical galaxies at $z = 1$.

Combining cosmic shear measurements of all “halos”, one can measure the lensing power spectrum Cl , where l is the multipole. The statistical error in Cl , assuming Gaussianity, is

$$\Delta Cl = \sqrt{\frac{2}{(2l+1)\Delta l f_{\text{sky}}}} \left(Cl + \frac{4\pi f_{\text{sky}}\sigma\epsilon^2}{Ng} \right). \quad (7)$$

Here, the first term is the cosmic variance and the second term is the shot noise, f_{sky} is the sky coverage and Δl is the size of the l bin, Ng is the number of 21cm absorption “halos”. Since we measure the shear averaged over the size of each 21cm absorption “halo”, one should replace Cl with the smoothed $\tilde{Cl} = Cl W^2\theta(l)$, with $W\theta$ being the Fourier transform of the window function describing each 21cm absorption region used for lensing measurement.

For a lower mass cut $7 \times 10^7 M_\odot$, there are about 10^6 first galaxies and thus 10^6 21cm absorption “halos” across the sky at $24 < z < 26$. The shot noise power spectrum is proportional to the square of $\eta \equiv \sigma\epsilon/Ng^{1/2}$. With $\sigma\epsilon \sim 0.1$ and $Ng \sim 10^6$, the typical value of η is 10^{-4} , for which precision measurement can be done up to $l \sim 5000$ (several arc-minute scale; Fig.3).

The lensing reconstruction from 21cm “halos” can be

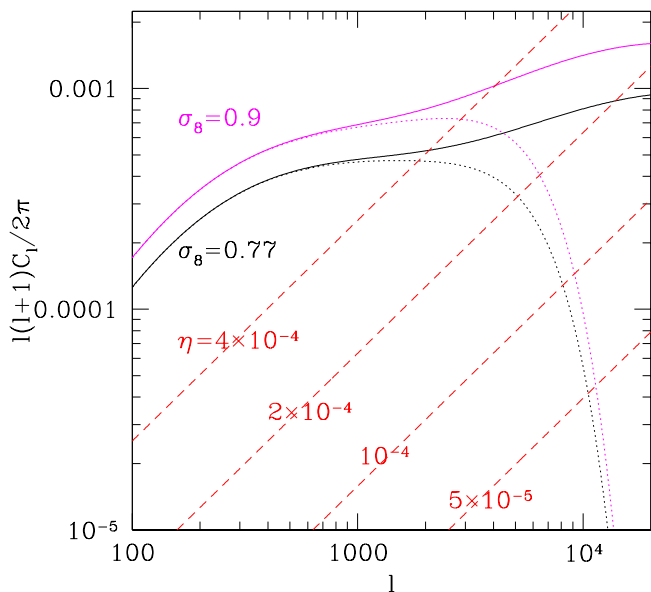


Figure 3. Error forecast for lensing power spectrum from shear measurement of $z \sim 25$ 21cm absorption “halos”. The solid curves are the lensing power spectra (without smoothing) at $z = 25$ for $\sigma_8 = 0.77$ and $\sigma_8 = 0.9$, respectively. Dashed lines are statistical error caused by shot noises as a function of $\eta \equiv \sigma\epsilon/Ng^{1/2}$, which is $\sim 10^{-4}$ for typical values of $\sigma\epsilon \sim 0.1$ and $Ng \sim 10^6$ with $\Delta l = 0.1l$ adopted. The quadrupole moment shear estimator measures the mean shear averaged over an aperture and allows the reconstruction of lensing at $l \lesssim 5000$ (dot lines, with smoothing area 4 arcmin^2). Small scale lensing power $l \gtrsim 5000$ can not be measured by the quadrupole moments shown here. However, it can be recovered by higher order moments such as the octopole moments. Eventually, one can recover all lensing information up to the limit of shot noise.

further improved. Figure 3 shows that there is significant power at small scales ($l \gtrsim 5000$). Since the quadrupole moment shear estimator only measures the averaged shear, the smoothing effect caused by the arcminute size of the smoothing area does not allow the extraction of small scale lensing information. By measuring higher order moments, however, smaller scale lensing information can be recovered. In the literature, the octopole moments have been proposed to measure the gradients of shear, or equivalently, the local shear (e.g., Goldberg & Natarajan 2002). The relative large size of 21cm absorption “halos” will make this measurement much easier than that of $z \sim 1$ galaxies. Eventually, by measuring all necessary moments, one can recover all lensing information up to the limit of shot noise. This will allow the measurement of the lensing signal to $l \sim 10^4$ (Fig. 3).

In the above estimation, we have assumed that intrinsic ellipticities do not correlate over relevant scales and thus only contribute to shot noise. This is obviously true for that induced by local processes discussed in previous sections, such as local density inhomogeneities and spin temperature anisotropy caused by the central sources. Could a fluctuating large scale field coupled to the brightness temperature, such as the fluctuating soft X-ray background (e.g.

Pritchard & Furlanetto 2007), invalidate the above assumption? The answer is probably no. The modes capable of inducing ellipticities must be smaller than the $\sim \text{Mpc}$ size of 21cm absorption “halos”. On the other hand, the modes capable of inducing correlations in intrinsic ellipticities are of size $\sim 2 \times 10^4/l h^{-1} \text{ Mpc}$. Thus a fluctuating background can only induce correlations in intrinsic ellipticities for those modes of $l > 10^4$, which are of little relevance to this paper.

In the directions along the line of sight and perpendicular to the line of sight, 21cm absorption halos may appear different, due to the evolution of these halos and the light cone effect, the redshift distortion, the beam and foreground (which are frequency and thus redshift dependent), etc. However, these physics do not induce asymmetry in the 2D plane perpendicular to the line of sight. Since we only use the shape distortion in the same 2D plane to measure cosmic shear, these physics do not induce systematics in the shear measurement.

Thus, with reasonable estimation of the 21cm absorption “halo” signal at high redshifts, rather conservative estimates for the intrinsic ellipticities caused by initial anisotropic Lyman- α emission from galaxies and reasonable estimates on the level of foreground induced ellipticity, the weak lensing application of these “halos” are very promising. The combined lensing S/N of $\sim 10^6$ 21cm “halos” at $z = 24 - 26$ is comparable to those with traditional cosmic shear measurements, with cosmic magnification of 21cm emitting galaxies, and with CMB lensing and 21cm background lensing.

7 SUMMARY AND DISCUSSION

In this paper, we investigate the potential of using 21cm absorption “halos” of first galaxies at $z \sim 25$ as background sources for gravitational weak lensing reconstruction. We show that the accuracy obtained using this method can be comparable, and may be superior, to some of the conventional methods. It is potentially very rewarding scientifically to detect and survey the first galaxies using future 21cm radio experiments for this and other applications.

There are several major uncertainties that may affect the results in this paper. The first one is the star formation efficiency c_* in large halos at $z \sim 25$. We have adopted $c_* = 0.2$ in the calculation. A smaller c_* would reduce the signal and size of the 21cm “halos” and thus make the observations and shear measurement more difficult. We have checked that adopting $c_* = 0.1$ doubles the r.m.s. of the ellipticity induced by the system noise for the same noise level $\sigma T = 7 \text{ mK}$. Secondly, there are uncertainties in the hard X-ray heating, which depends on the energy extraction efficiency from black holes and the fraction of the released energy in the form of hard X-rays (see Cen 2006 for more details). If the real values are lower than what are adopted in our calculation, the X-ray heating would be less important and the 21cm absorption “halos” may form at redshifts lower than $z = 25$. As a consequence, we would have much more observable 21cm absorption “halos” and the statistical errors of the lensing measurement would be significantly improved. If the X-ray heating is more efficient than we assume, the detection of 21cm absorption “halos” would be more demanding and it becomes more difficult to use these

“halos” for the lensing application. To reduce the above two types of uncertainties, we have to advance our understanding of the formation of the first objects. On the other hand, the observation (or even null observation) of the 21cm absorption “halos” would lead to valuable constraints on star formation and X-ray heating at $z \sim 20-30$. Lastly, we have neglected any errors in the shear measurement induced by map making. Although in principle these errors can be corrected (Chang et al. 2004), it is not clear how well the correction is for unprecedented radio arrays required for 21cm absorption “halo” observations. The discussion of such residual errors is certainly beyond the scope of this paper.

While we focus here on the weak lensing application of the 21cm absorption “halos”, because of their arc-minute size and high redshifts, these “halos” also have interesting strong lensing signatures, which is discussed in Li et al. (2007).

ACKNOWLEDGMENTS

We thank Gary Bernstein, Xuelei Chen, Leonid Chuzhoy, Bhuvnesh Jain, Yipeng Jing, Jordi Miralda-Escudé and Zhiqiang Shen for helpful discussions. We thank Ue-Li Pen and Olivier Zahn for valuable information on observations. PJZ is supported by the One-Hundred-Talent Program of Chinese academy of science and the NSFC grants (No. 10543004, 10533030). ZZ acknowledges the support of NASA through Hubble Fellowship grant HF-01181.01-A awarded by the Space Telescope Science Institute, which is operated by the Association of Universities for Research in Astronomy, Inc., for NASA, under contract NAS 5-26555. RC is supported in part by grants AST-0407176 and NNG06GI09G.

REFERENCES

Alcock, C., & Paczyński, B. 1979, *Nature*, 281, 358

Bartelmann, M., & Schneider, P. 2001, *Physics Report*, 340, 291

Bowman, J. D., Morales, M. F., & Hewitt, J. N. 2006, *ApJ*, 638, 20

Cen, R. 2006, 2006, *ApJ*, 648, 47

Chang, T.-C., Refregier, A., & Helfand, D. J. 2004, *ApJ*, 617, 794

Chen, X., & Miralda-Escudé, J. 2006, *astro-ph/0605439*

Chuzhoy, L., Alvarez, M. A., & Shapiro, P. R. 2006, *ApJ*, 648, L1

Chuzhoy, L., & Shapiro, P. R. 2006, *ApJ*, 651, 1

Cooray, A. 2004, *New Astron. Rev.* 9, 173

Dodelson, S., Shapiro, C., & White, M. 2006, *PRD*, 73, 023009

Eisenstein, D. J., et al. 2005, *ApJ*, 633, 560

Field, G. B., 1959, *ApJ*, 129, 551

Goldberg, D. M., & Natarajan, P. 2002, *ApJ*, 564, 65

Goldberg, D. M., & Bacon, D. J. 2005, *ApJ*, 619, 741

Hoekstra, H., et al. 2006, *ApJ*, 647, 116

Hu, W. 2001, *PRD*, 64, 083005

Hu, W. & Okamoto, T. 2002, *ApJ*, 574, 566

Jarvis, M., Jain, B., Bernstein, G., & Dolney, D. 2006, *ApJ*, 644, 71

Keshet, U., Waxman, E., & Loeb, A. 2004, *ApJ*, 617, 281

Li, G., Zhang, P., & Chen, X. 2007, *ArXiv Astrophysics e-prints*, arXiv:astro-ph/0701492

Mandel, K.S. & Zaldarriaga, M. 2006, *ApJ*, 647, 719

Peacock, J. A., & Dodds, S. J. 1996, *MNRAS*, 280, L19

Pen, U. 2004, *New Astronomy*, 9, 417

Peterson, J.B., Bandura, K. & Pen, U.L., 2006, *astro-ph/0606104*

Pritchard, J.R., Furlanetto, S.R., 2007, *MNRAS*, 376, 1680

Refregier, A. 2003, *ARAA*, 41, 645

Seljak, U. & M. Zaldarriaga, 1999, *PRL*, 82, 2636

Sheth, R. K., & Tormen, G. 2002, *MNRAS*, 329, 61

Sigurdson, K., & Cooray, A. 2005, *PRL*, 95, 211303

Spergel, D.N. et al. 2006, *astro-ph/0603449*

Thompson A.R., Moran, J.M. & Swenson, G.W. Jr., 2001, *Interferometry and synthesis in radio astronomy*, 2nd. ed., Wiley, New York

Upadhye, A., Ishak, M., & Steinhardt, P. J. 2005, *PRD*, 72, 063501

Van Waerbeke, L., Mellier, Y., & Hoekstra, H. 2005, *Astronomy and Astrophysics*, 429, 75

Wang, X., Tegmark, M., Santos, M., Knox, L. 2006, *ApJ*, 650, 529

Wouthuysen, S. A., 1952, *AJ*, 57, 31

Zahn, O. & Zaldarriaga, M. 2006, *ApJ*, 653, 922

Zaldarriaga M. & Seljak, U., 1999, *PRD*, 5913507

Zhang, P.J. & Pen, U.L. 2005, *PRL*, 95, 241302

Zhang, P.J., & Pen, U.L. 2006, *MNRAS*, 367, 169

Zheng, Z., & Miralda-Escudé, J., 2002, *ApJ*, 578, 33